

Wind and rain compound with tides to cause frequent and unexpected coastal floods

Thomas Thelen^{1,*}, ththelen@ncsu.edu, <https://orcid.org/0000-0003-2993-6446>

Katherine Anarde¹, kanarde@ncsu.edu, <https://orcid.org/0000-0003-2586-0587>

Joel Casey Dietrich¹, jcdietrich@ncsu.edu, <https://orcid.org/0000-0001-5294-2874>

Miyuki Hino^{2,3}, mhino@unc.edu, <https://orcid.org/0000-0001-9369-5769>

¹ Department of Civil, Construction, and Environmental Engineering, North Carolina State University, 915 Partners Way, Raleigh, NC, USA

² Department of City and Regional Planning, University of North Carolina at Chapel Hill, 223 E Cameron Avenue, Chapel Hill, NC, USA

³ Environment, Ecology, and Energy Program, University of North Carolina at Chapel Hill, 121 South Road, Chapel Hill, NC, USA

*Corresponding author

Abstract

With sea-level rise, flooding in coastal communities is now common during the highest high tides. Floods also occur at normal tidal levels when rainfall overcomes stormwater infrastructure that is partially submerged by tides. Data describing this type of compound flooding is scarce and, therefore, it is unclear how often these floods occur and whether there are other non-tidal factors that contribute to flooding. We combine measurements of flooding on roads and within storm drains with a numerical model to examine processes that contribute to flooding in Carolina Beach, NC, USA – a community that chronically floods outside of extreme storms despite flood mitigation infrastructure to combat tidal flooding. Of the 43 non-storm floods we measured during a year-long study period, one-third were unexpected by the community because the forecasted tide was below their monitoring threshold. We introduce a novel model coupling between an ocean-scale hydrodynamic model (ADCIRC) and a community-scale surface water and pipe flow model (3Di) to quantify contributions from multiple flood drivers. We find that setup from sustained (non-storm) winds modulates flood extents and depth: wind setup causes deeper, longer, more extensive flooding during the highest high tides and can cause floods on days when flooding would not have occurred due to tides alone. Rainfall also contributes to unexpected floods; because tides submerge stormwater outfalls on a daily basis, even minor rainstorms lead to flooding as runoff has nowhere to drain. As a particularly low-lying coastal community, Carolina Beach provides a glimpse into future challenges that coastal communities worldwide will face in predicting, preparing for, and adapting to increasingly frequent flooding from compounding tidal and non-tidal drivers atop sea-level rise.

Keywords

coastal flooding, sea-level rise, high-tide flooding, compound flooding, hydrodynamic modeling, climate adaptation

1. Introduction

As sea levels continue to rise, coastal floods are occurring more frequently even in the absence of extreme storms (Sweet et al., 2022). Marine water levels overtop low-lying shorelines and backflow into stormwater infrastructure (pipes and ditches) during the highest high tides, flooding roads and other low-lying areas (Sweet et al., 2018). Flooding also occurs during normal tidal levels due to impaired stormwater infrastructure: with reduced capacity to convey runoff, everyday rainstorms can overcome submerged or partially full stormwater networks, leading to flash floods (Gold et al., 2023; Sadler et al., 2020). Sea-level rise (SLR) has also elevated shallow groundwater tables, reducing infiltration of rainfall runoff on the surface and increasing rates of infiltration into stormwater drainage networks in the subsurface (Befus et al., 2020; Bosserelle et al., 2022). These land-based drivers complicate the usage of terminology used to describe flooding from SLR (e.g., “high-tide flooding” or “sunny-day flooding”). Here, we use the terms “chronic coastal flooding” (Hague et al., 2023) or “chronic flooding” (Thiéblemont et al., 2023), to include all recurrent coastal floods occurring outside of extreme storms (i.e., named tropical storms and Nor’easters) due to both marine (e.g., tides, wind, atmospheric pressure) and land-based drivers (e.g., rain, impaired stormwater networks, groundwater) acting atop higher sea levels.

Evidence of the frequency, spatial extent, and mechanisms driving chronic coastal flooding is scarce. Due to data availability, previous work has largely focused on contributions to floods from marine sources. Analysis of tide gauge data has shown that ocean-scale processes like wind setup, circulation patterns, and thermal expansion combine with tides to elevate water levels along the coast (Li et al., 2022). These “non-tidal residuals” contribute significantly to marine water levels during high-tide floods along the East Coast of the United States (Li et al., 2022), and are incorporated in high-tide flood predictions made at tide gauges (Dusek et al., 2022). Tide gauges, however, are geographically sparse. They are also located over marine water bodies and therefore cannot capture localized, land-based flood drivers, which cause variations in flooding on the scale of city blocks (Shen et al., 2019). Flood data from in-situ sensors on land have been limited in space and time, restricted to a few communities and characterized by short time records (Gold et al., 2023; Mydlarz et al., 2024; Silverman et al., 2022). More data and new methods are needed to quantify the relative importance of land and marine-based flood drivers to chronic coastal floods at a block-by-block scale.

The most common approach for investigating the spatial extent and depth of chronic coastal flooding is “bathtub” modeling, where all elevations below a given water level are considered inundated (e.g., Gold et al., 2022; Williams and Lück-Vogel, 2020; Yunus et al., 2016). Because this method combines all flood drivers into one total water level term, it cannot resolve interactions between multiple flood drivers, nor interactions with infrastructure, which cause more complex flood patterns. In contrast to bathtub modeling, combined surface water and pipe flow models capture interactions between land and marine-based drivers. Numerical models that couple 1D pipe flow simulations and 2D surface flow simulations are used to simulate multi-driver flooding in urban areas (e.g., Fan et al., 2017; Seyoum et al., 2012). However, their application to coastal flooding is less common (Sadler et al., 2020; Shen et al., 2019; Zahura and Goodall, 2022). While 1D-2D models of chronic coastal flooding have the potential to resolve multiple flood drivers interacting with infrastructure, model results in coastal systems have not been validated against direct measurements of flooding on land, nor have the models been adapted to analyze the contributions of flood drivers acting over multiple spatial scales (e.g., rainfall runoff within a city block versus wind setup acting over a long fetch).

A growing body of literature has identified impacts of chronic coastal floods to people, businesses, and communities, with impacts spanning traffic delays (Hauer et al., 2023), water quality risks (Carr et al., 2024; Macías-Tapia et al., 2021), reduced economic activity (Hino et al., 2019), property damage (Moftakhari et al., 2018), and changing development patterns (Buckman and Sobhaninia, 2022). Given the limited data describing this type of flooding and the lack of validated models capable of resolving flood drivers at relevant spatial and temporal scales, relating impacts to flood mechanisms remains difficult, constraining our understanding of the social and economic burden of these floods. Uncertainty in the relative importance of tidal versus non-tidal flood drivers also hampers flood prediction and community preparedness for floods, particularly in regions far from tide gauges.

We combine land-based flood measurements with a new coupled hydrodynamic and stormwater model to examine variability in processes that drive chronic flooding in a coastal community over seasonal timescales, and relate this understanding to how communities prepare for flooding outside of extreme storms. Our analysis focuses on the Town of Carolina Beach, North Carolina (NC), USA, a coastal community that employs preventative infrastructure

1
2
3
4 and flood monitoring thresholds to try to minimize impacts from chronic flooding. We find that
5 one-third of measured floods occurred at forecasted tides below the community's flood
6 monitoring threshold because of contributions from wind, rain, and impaired stormwater
7 networks. We place our findings in context of how low-lying coastal communities may use local
8 knowledge of the relative importance of different flood drivers to better prepare for current and
9 future flood hazards.
10
11

12 13 2. *Methods*

14 2.1 *Study location*

15
16 The Town of Carolina Beach sits between the Cape Fear River Estuary to the west and
17 the Atlantic Ocean to the east (Fig. 1A). North of the Town, these two water bodies connect via
18 a man-made waterway (Snow's Cut, part of the Intracoastal Waterway) and a tidal inlet. The
19 Yacht Basin is a dredged back-bay that extends south into the Town from the Intracoastal
20 Waterway. Flooding occurs regularly on Canal Drive, a low-lying road running along reclaimed
21 land on the eastern edge of the Yacht Basin (Fig. 1B). During these chronic flood events, water
22 from the Yacht Basin propagates up through subterranean stormwater infrastructure to flood the
23 road, often prior to the overtopping of bay shorelines and bulkheads.
24
25

26 The Town of Carolina Beach has sought to mitigate flooding emanating from the
27 stormwater system through installation of backflow prevention devices on stormwater outfalls to
28 the Yacht Basin located at each intersection along Canal Drive (e.g., Fig. 1C). These devices
29 include inline check valves and external "duckbill" devices designed to allow only one-way flow;
30 when functioning as intended, these devices prevent water from entering the stormwater system
31 from the Yacht Basin during high water levels while allowing water to exit the pipes during low
32 water levels. The Town's stormwater network is disconnected, so backflow prevention from
33 each of these devices is localized to clusters of catch basins and pipes that drain individual
34 intersections (e.g., Fig. 1C).
35
36

37 Individual homeowners also employ localized flood mitigation through construction of
38 bulkheads. Bulkheads along Canal Drive vary in elevation and are not continuous. A 2019
39 Flooding and Vulnerability Study (APTIM, 2019) documented bulkheads installed on 89% of the
40 144 lots surrounding the Yacht Basin. However, it is unclear how much flooding along Canal
41 Drive stems from overtopping of low-lying shorelines (around/over bulkheads) compared to the
42 failure of backflow prevention devices (due to biofouling, debris, or groundwater bypassing).
43
44

45 The Town regulates access to Canal Drive during floods through a series of gates
46 restricting access to the road. Decisions to close the gates are made using local forecasts of
47 peak astronomical tides. If the forecasted tide exceeds 1.83 m (6 ft) Mean Lower Low Water
48 (MLLW) the gates are lowered. These highest high tides occur during, for example, perigean
49 spring tides, when the moon, earth, and sun are in alignment, and the moon is closest in its orbit
50 to earth. If the forecasted tide is between 1.83 and 1.60 m MLLW, Town staff monitor Canal
51 Drive in person and close the road if flooding is observed. Canal Drive is not monitored if the
52 forecasted tide is less than 1.60 m (5.25 ft) MLLW, except when strong northerly winds are
53 forecast which Town staff know anecdotally can elevate water levels in the Yacht Basin. Despite
54 local knowledge of the importance of wind to flooding, there are currently no thresholds for wind
55 intensity or direction included in Town decision-making for road closures. This is largely due to a
56 lack of systematic knowledge of flood drivers and a lack of information on non-tidal drivers
57
58
59
60
61
62
63
64
65

tailored to the needs of Town staff. In the following sections, we describe a two-pronged approach – developed in collaboration with Town officials – which combines measured data and numerical modeling to improve understanding of factors that lead to flooding.

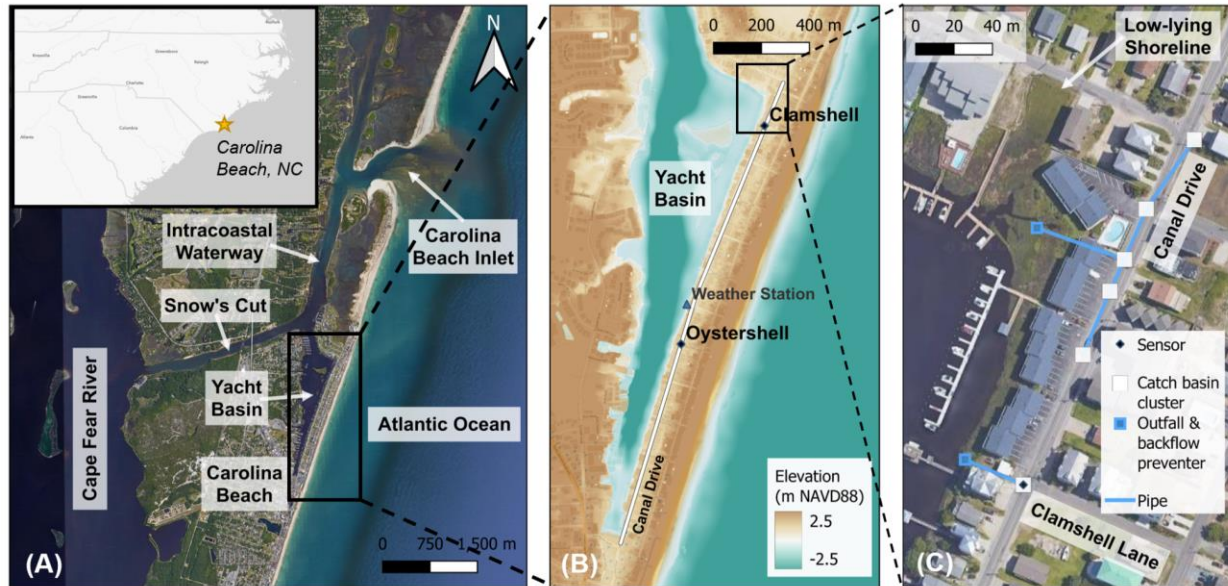


Figure 1. (A) Carolina Beach study site and neighboring water bodies. (B) Elevation map (Coastal National Elevation Database; Thatcher et al., 2016) of the study site (black box in A), including the location of Clamshell Lane and Oystershell Lane flood sensors that measure water levels and collect images of flood extent along Canal Drive (black diamonds) and the Town-operated weather station (blue triangle). (C) Zoomed-in view of the stormwater infrastructure along the north end of Canal Drive (black box in B). The stormwater infrastructure at all other cross-streets intersecting Canal Drive is similar to the Clamshell Lane intersection with Canal Drive in (C), where clusters of catch basins drain directly to the Yacht Basin without any additional subterranean (pipe) connections along Canal Drive

2.2 In-situ measurement of flood incidence and extent

We worked with Town officials to instrument flood hotspots along Canal Drive with Sunny Day Flooding Sensors (SuDS; Gold et al., 2023). Each SuDS installation consists of a pressure sensor installed in a stormwater catch basin and a co-located sub-aerial gateway with a camera. Collectively, the sensors transmit water levels and roadway images every six minutes to a web application, which serves as a real-time indicator for the Town of flood incidence and spatial extent (Hayden-Lowe et al., 2022). The sensors were validated through comparison with an in-situ commercial water level sensor (Supplementary Fig. S.9).

This paper uses data from the two sensors with the longest data records: the sensor at the intersection of Canal Drive and Clamshell Lane, and the sensor at the intersection of Canal Drive and Oystershell Lane (Fig. 1B; referred to as the “Clamshell” and “Oystershell” sensors). Measurements span April 1, 2022 to April 24, 2023 at the Clamshell sensor and June 2, 2022 to April 24, 2023 at the Oystershell sensor. Intermittent sensor outages occurred due to issues with batteries and sensor housing leaks. Water levels were recorded for 76% of the study

1
2
3
4 periods at the two sensors (Supplementary Table S.3). There were fewer data gaps in the
5 imagery record; we recorded images for 95% of the study period at the Clamshell location and
6 99% of the study period at the Oystershell location.
7

8 We use the in-situ water levels and camera imagery to assess flood incidence and to
9 validate the numerical model. We define a flood as occurring when water levels surpass the
10 elevation of the top of the catch basin grate, which are immediately adjacent to the road at both
11 sensor locations. While this threshold differs from the 3-cm depth threshold proposed by
12 Mofstakhari et al. (2018) – which was specified to account for digital elevation map uncertainty in
13 mapping of tidal flooding – we consider any amount of water on the road as a potential flood
14 impact because even small puddles of saltwater can splash onto the underside of vehicles and
15 cause corrosion. For our analysis, a flood ends when water levels recede below the top of grate
16 elevation. Flood magnitude is calculated as the maximum water depth above the edge of the
17 road.
18
19
20
21

22 *2.3 Wind and rain measurements*

23 A weather station in the Yacht Basin (Fig. 1B) records 10-minute wind speed and
24 direction, and rain accumulation measured every minute. It also records water levels in the
25 Yacht Basin at intervals of no longer than 10 minutes. Wind speeds measured at the station are
26 lower than what would be measured on the open coast because the Yacht Basin is ringed by
27 structures that block wind. Wind speed and direction associated with a flood are averaged over
28 the 24 hours preceding each event because sensitivity testing with different averaging intervals
29 shows this interval balances over-smoothing longer-term changes in wind direction with
30 misrepresenting shorter-term changes in wind speed. To calculate the rain accumulation
31 associated with a flood, we consider the duration of the flood and the two hours prior, thereby
32 capturing the upper half of the rising tide that inundates stormwater outfalls and impedes
33 drainage.
34
35
36
37
38

39 *2.4 Multi-driver flood model*

40 Data on flood incidence and depth are used to validate a numerical model capable of
41 simulating water level contributions from multiple drivers. The flood model consists of an ocean-
42 scale circulation model that is one-way coupled to a community-scale flood model. Collectively,
43 the coupled model can simulate tides, atmospheric conditions (air pressure and wind), rainfall
44 runoff, pipe flow, surface water flow, and the effects of infrastructure like backflow prevention
45 devices and bulkheads. In the sections that follow, we summarize model components and
46 coupling.
47
48
49

50 *2.4.1 Ocean-scale circulation model: ADCIRC*

51 We use the Advanced Circulation Model (ADCIRC; Luettich et al., 1992; Westerink et al.,
52 1992) to simulate offshore and nearshore drivers of coastal water levels. ADCIRC uses
53 unstructured meshes to represent complex coastal environments and predict the effects of
54 tides, winds, and river flows on water levels and depth-averaged currents. Our ADCIRC
55 simulations are performed using the NC Coastal Flood Analysis System Model Grid (Blanton
56 and Luettich, 2008), which covers the Western North Atlantic Ocean. The mesh was designed
57 for floodplain mapping and storm surge prediction in NC; therefore, its highest resolution is
58
59
60
61
62
63
64
65

1
2
3
4 along the NC coast and surrounding floodplains (approx. 40 m to 150 m). To improve the
5 representation of topography and bathymetry near our study site, we interpolated elevations
6 reported in the Coastal National Elevation Database (CoNED; Thatcher et al., 2016) to the
7 ADCIRC mesh around Carolina Beach.
8

9 Tides with four diurnal (K1, O1, P1, and Q1) and semidiurnal (M2, S2, N2, and K2)
10 constituents are applied as periodic forcing at the open ocean boundary and as potentials
11 throughout the model domain. Atmospheric forcing consists of wind speed and air pressure data
12 from the North American Mesoscale (NAM) Forecast System Analysis product (Rogers et al.,
13 2009) interpolated at three-hour intervals from the 12-km NAM product grid to the ADCIRC
14 mesh. All simulations include a seven-day ramp for tidal and atmospheric forcings.
15
16

17 Lastly, we set a global water level offset in ADCIRC to account for seasonal water level
18 fluctuations that are not captured in the atmospheric forcing (e.g., thermal expansion – Asher et
19 al., 2019). This offset was calculated by comparing model output prior to a flood with
20 measurements of water levels from the Yacht Basin weather station (Supplementary Eqn. S.1).
21
22

23 *2.4.2 Community-scale flood model: 3Di*

24 We couple ADCIRC with the hydrodynamic model 3Di (Stelling, 2012) to simulate land-
25 based flood drivers, including pluvial flooding (i.e., rainfall) and the effects of stormwater
26 infrastructure (i.e., pipe networks and backflow prevention devices). 3Di simulates one-
27 dimensional pipe flows (Casulli and Stelling, 2013), two-dimensional surface water flows
28 (Casulli, 2009; Casulli and Stelling, 2011), and their interactions, resulting in a mass-
29 conservative simulation of free surface and pipe flows. 3Di has been used previously to map
30 SLR and storm inundation (Ju et al., 2017). This is the first coupling of 3Di with ADCIRC.
31
32

33 The 3Di model domain includes the land and waterways in and around Carolina Beach
34 (area within the white and orange outlines in Fig. 2). The 3Di subgrid calculation method
35 enables calculated water depths to vary at the resolution of the input elevation raster (Casulli
36 and Stelling, 2011; Volp et al., 2013) such that simulated flood extents and depths reflect small
37 variations in topography. We use the 1-m horizontal resolution CoNED digital elevation model
38 (Thatcher et al., 2016) as the elevation raster input for 3Di. The calculation grid resolution is
39 shown in Figure 2, with the highest resolution (12 m) in the Yacht Basin, nearby channels,
40 nearshore ocean, and along Canal Drive. Bottom friction is represented with Manning's n values
41 converted from a land-cover data set (Dietrich et al., 2011; Office for Coastal Management,
42 2022). Pluvial contributions to flooding are simulated using five-minute rainfall measured at the
43 weather station (Fig. 1B) applied as a spatially constant input. Because the study area is heavily
44 developed with extensive impervious or low-infiltration surfaces and the groundwater table is
45 high in low-lying coastal areas (Bosserele et al., 2022), we assume no infiltration in 3Di
46 simulations.
47
48

49 Stormwater infrastructure along Canal Drive is represented in 3Di by 1D flow features.
50 Each inlet cluster at a Canal Drive intersection is modeled using a single catch basin node at
51 the lowest point of the 12 m calculation cell. Bulkheads are modeled as linear obstacles, with
52 elevations sourced from the Flooding and Vulnerability Study (APTIM, 2019). To simulate the
53 effect of backflow prevention devices in the subterranean pipe network, we apply 1D weir
54 equations at the outfall from the catch basin nodes to the Yacht Basin. We tune the loss
55 coefficients in the weir equations (Supplementary Eqn. S.2) to best match the hydrographs
56
57
58
59
60
61
62
63
64
65

measured by the in-situ flood sensors (Supplementary Fig. S.4). This parameterization of the backflow prevention devices incorporates site-specific processes because our measured water levels in the catch basins are influenced by 1) processes that reduce the effectiveness of the backflow prevention devices, like biofouling; and 2) infiltration of groundwater via cracks in the stormwater network.

2.4.3 Model coupling

The coupling between ADCIRC and 3Di is one-way, meaning that ADCIRC water levels are boundary conditions for the 3Di model. Two-minute interval water level time series interpolated from ADCIRC force surface water flows at the 3Di model boundaries (orange lines in Fig. 2). The final simulation product from the coupled “flood model” are water depths resolved at a six-minute temporal resolution and one-meter spatial resolution on land and within subterranean stormwater infrastructure.

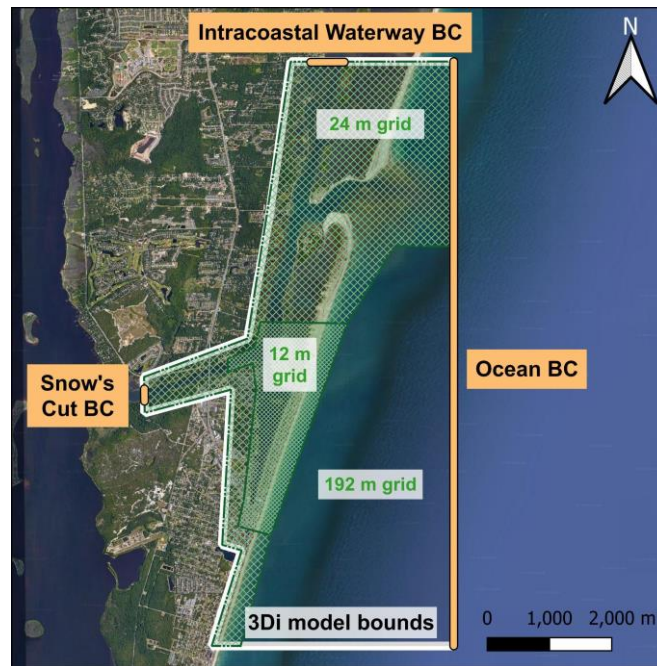


Figure 2. 3Di model domain and grid resolution. The boundaries used for the one-way coupling from ADCIRC to 3Di are shown in orange.

2.5 Modeled decomposition of flood drivers

We developed the flood model to better understand the relative contributions of tides, atmospheric conditions, and rainfall to total water levels on land and in stormwater infrastructure during flood events. We compare three model simulations for each hindcast flood event, with each simulation incorporating additional forcing. The first model simulation includes only tidal forcing (referred to as the “tides” simulation). The second model simulation includes both tidal and atmospheric forcings from ADCIRC, including the effects of pressure and wind (the “tides+atmospheric” simulation). The third simulation includes three forcings: tides and atmospheric forcing in ADCIRC plus rainfall in 3Di (the “tides+atmospheric+rainfall” simulation). Water levels from the tides, atmospheric, and rainfall simulation are compared to measured

water levels at the Clamshell and Oystershell catch basins for three hindcast flood events (Table 2) for model validation. The influence of individual flood drivers is then found by differencing these model simulations as shown by the driver decomposition formulations in Table 1.

Table 1. Formulations used to decompose modeled water level contributions from tides, atmospheric conditions, and rainfall during hindcast flood events.

Flooding driver	Water level time series decomposition to isolate driver contribution
Tides	(tides simulation)
Atmospheric conditions	(tides+atmospheric simulation) <i>minus</i> (tides simulation)
Rainfall	(tides+atmospheric+rainfall simulation) <i>minus</i> (tides+atmospheric simulation)

3. Results

3.1 Flood measurements and community response

From April 1, 2022 to April 24, 2023, we recorded 56 instances of water levels above the roadway in Carolina Beach (at the Clamshell sensor, Fig. 1, which is the longest data record). Ten floods identified using imagery alone are excluded from Fig. 3 because we do not have water level measurements due to pressure sensor outages. We also exclude three floods that occurred during Hurricane Ian (September 29-30, 2022; Fig. 3A), the only named storm that made landfall in the mid-Atlantic during the study period. As in Gold et al. (2023), we categorize the remaining 43 chronic floods as “rainy-day” floods – that is, floods that coincided with a rain event – or “sunny-day” floods – floods that occurred with no measured precipitation. Using this nomenclature, we observed 28 sunny-day floods (Fig. 3B, yellow circles) and 15 rainy-day floods (Fig. 3B, teal triangles). Rain accumulation varied from 0.2 mm to 37.6 mm (Fig. 3B, size of teal triangles). We find that rainy-day floods were typically longer in duration, for the same flood magnitude, than sunny-day floods.

Over the study period, 33% of chronic floods (14 of 43 floods) occurred during forecasted tides below the Town’s monitoring threshold, meaning these floods were largely unexpected (Fig. 3C). Comparison of tidal and meteorological data indicates that all 14 unexpected floods occurred during a rising or high tide accompanied by northeasterly winds, rainfall, or a combination of the two (Fig. 3D). Eleven of the 14 unexpected floods occurred during a northeasterly wind (orange circles and triangles in the upper right quadrant of Fig. 3D), with wind speeds ranging from 2.2 m/s to 6.8 m/s (averaged over the 24 hours preceding the event). Winds out of the northeast align with the long axis of the Yacht Basin and the Intracoastal Waterway to the north (Fig. 1A). Of the 11 unexpected floods concomitant with a northeasterly wind, four were also accompanied by rainfall. The remaining 3 unexpected floods that occurred without northeasterly winds were concomitant with rainfall (orange triangles, lower half of Fig. 3D).

The largest flood magnitudes (i.e., maximum depth at the sensor location) occurred when wind was northeasterly. For the six largest floods – the floods that exceed the 0.4-m radial axis line in Fig. 3D, which corresponds to flood magnitude – the same number occurred during

high tidal stages (black dot) and low tidal stages (orange triangle, denoting rain and northeasterly wind).

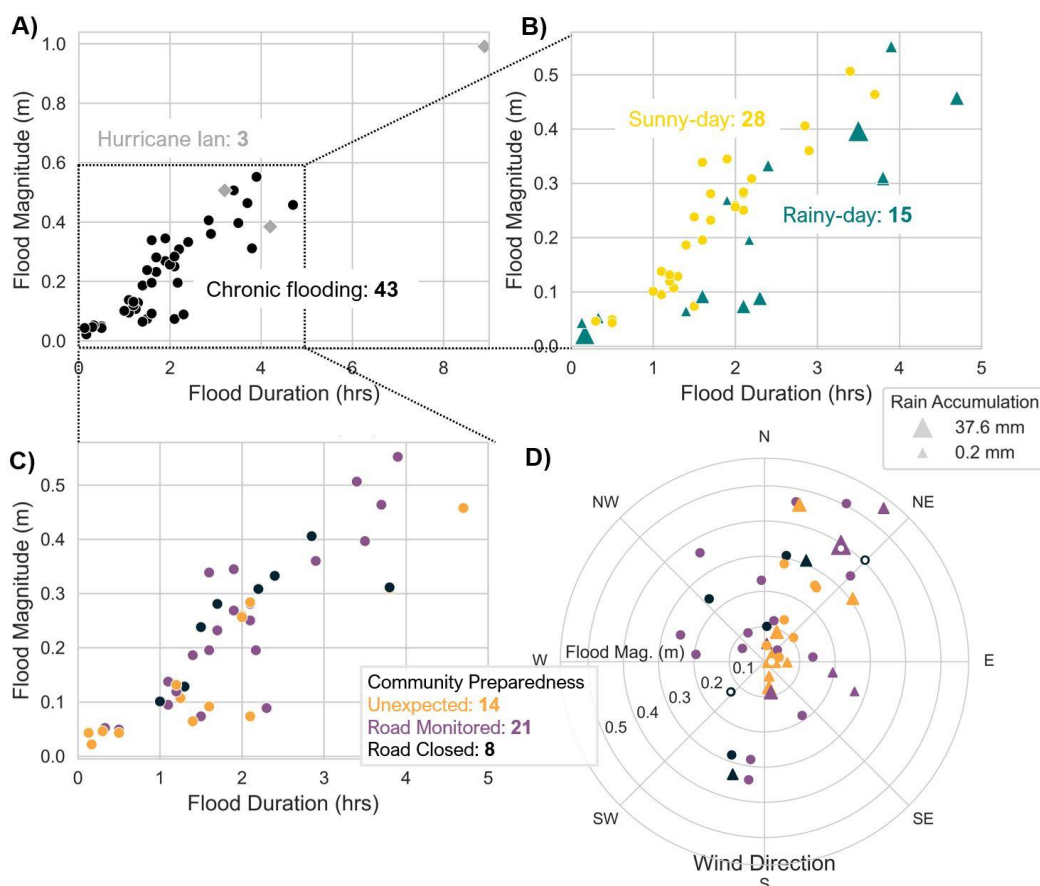


Figure 3. In-situ measurements of flood magnitude (maximum water depth on road) at the Clamshell sensor (Fig. 1, April 1, 2022 - April 24, 2023), plotted against flood duration (A-C) and wind direction (D). (B-D) examine only the “chronic floods” (black dots in A) that occurred outside of named extreme storms (gray diamonds in A). In (B), floods are classified as sunny-day floods (yellow circles) or rainy-day floods (teal triangles, where size scales with the magnitude of rain accumulation during the flood and the two preceding hours). In (C), floods are binned by the level of community preparedness for the flood: black indicates preemptive road closure (forecasted tide ≥ 1.83 m MLLW), purple indicates monitoring of road conditions (tide between 1.60 and 1.83 m MLLW), and orange indicates “unexpected” floods when the road was not monitored or closed (tide < 1.60 m MLLW). In (D), wind direction (where the wind was blowing from) is averaged over the 24 hours preceding the flood; the radial axis shows flood magnitude; the scaling of triangles shows rain accumulation as in (B); the point coloring shows community preparedness as in (C); and flood points with white interiors are modeled in Section 3.2.

3.2 Flood modeling and driver decomposition

We use the flood model to quantify contributions of individual flood drivers to flood magnitude, duration, and spatial extent for three measured flood events. These floods (points

with white centers in Fig. 3D) span different combinations of tidal and meteorological conditions, as well as community preparedness. Table 2 summarizes the forecasted tidal levels (i.e., used for monitoring and closing roads), actual community response (i.e., alerts and road closures), measured rain accumulation, and measured wind speed and direction for each flood. We refer to these flood events by the month and year that they occurred, and the hypothesized primary flood driver.

The “June 2022 perigean spring tide event” included two floods (June 14-15 and 15-16) during perigean spring tides. These floods co-occurred with the second (June 14-15) and fourth (June 15-16) highest forecasted tidal peaks of the year (NOAA, 2022). The community was alert to flooding during this event, as evidenced by pre-emptive road closures on Canal Drive and a “king tide” flood alert post on Facebook. Conversely, the “August 2022 rain event” occurred during one of the smallest forecasted tidal peaks of the month (NOAA, 2022). Road closure barriers were not placed on Canal Drive before or during this flood event, nor was there a social media alert. The forecasted tide during the “January 2023 mixed-drivers event” was higher than the August event but lower than the June event, within the monitoring range for road closure. For this event, barriers were placed on Canal Drive 30 minutes before the flood, but there was no social media alert. Imagery from the flood sensors during each event is included in the Supplement (Fig. S.5-8).

Table 2. The three measured flood events selected for modeling. The names associated with each flood event include the month that they occurred and the hypothesized primary flood driver.

Modeled flood events	June 2022 perigean spring tide event	August 2022 rain event	January 2023 mixed-drivers event
<i>Flood date or dates</i>	June 14-16	August 19	January 22
<i>Predicted high tide (m MLLW)</i>	1.92 m	1.37 m	1.77 m
<i>Community preparedness measures</i>	Pre-emptive social media post, road closure	None	Road closure as flooding started
<i>Measured rain accumulation</i>	None	33 mm over 2 hrs.	48 mm over 6 hrs.
<i>Measured wind speed and direction</i>	June 14-15: 3.3 m/s, 230°N June 15-16: 2.2 m/s, 40°N	1.9 m/s, 70°N	2.5 m/s, 30°N

In the sections that follow, we examine three simulations for each modeled flood event using the forcing combinations identified in Table 2: tides, tides+atmospheric, and tides+atmospheric+rainfall. First, we compare in-situ sensor data and modeled water levels from each event. Then, we examine trends spatially.

3.2.1 June 2022 perigean spring tide event

During the June 2022 perigean spring tide event, two floods were measured during the highest high tides each day: a smaller flood on the evening of June 14 and a larger flood on the evening of June 15 (dotted black lines in Fig. 4B). (At this time, the Oystershell sensor had not yet been installed, so only the Clamshell sensor is shown in Fig. 4). The measured water level time series for this event demonstrates how high water levels in the Yacht Basin – in the absence of rain – can cause flooding on Canal Drive. As bay water levels increase with a rising tide, stormwater outfalls become inundated, but backflow prevention devices slow the flow of bay water into the stormwater system (shown in Fig. 4B by the gradual increase in slope of the dotted line at the beginning of each rising tide). The Clamshell catch basin fills rapidly once water levels surpass the lowest-lying shoreline along the perimeter of the Yacht Basin and flow overland to Canal Drive; this phenomenon is visible in imagery and manifests in the measured water level time series by sudden increases in water level at 21:00 on June 14 and June 15.

The model indicates that atmospheric forcing contributed to roadway flooding during the June 2022 perigean spring tide event. Comparison of the tides+atmospheric and tides simulations show that atmospheric conditions reduced water levels (i.e., setdown) until the evening of June 15 (Fig. 4C, shown through a shift in atmospheric water level contributions from negative to positive). Thereafter, a change in wind direction – from southwesterly to northeasterly (Fig. 4A) – elevated water levels (i.e., setup), which when combined with tides, resulted in more flooding on the road (Fig. 4B). The flood model reproduces overland flooding at the Clamshell catch basin for the June 15-16 flood (Fig. 4B, rapid increase in the solid pink and dashed purple lines at 21:00 on June 15) but not for the June 14-15 flood, as modeled water levels in the Yacht Basin for the tides+atmospheric simulation were 0.1 m lower than measured water levels at the flood peak (see Supplementary Fig S.1).

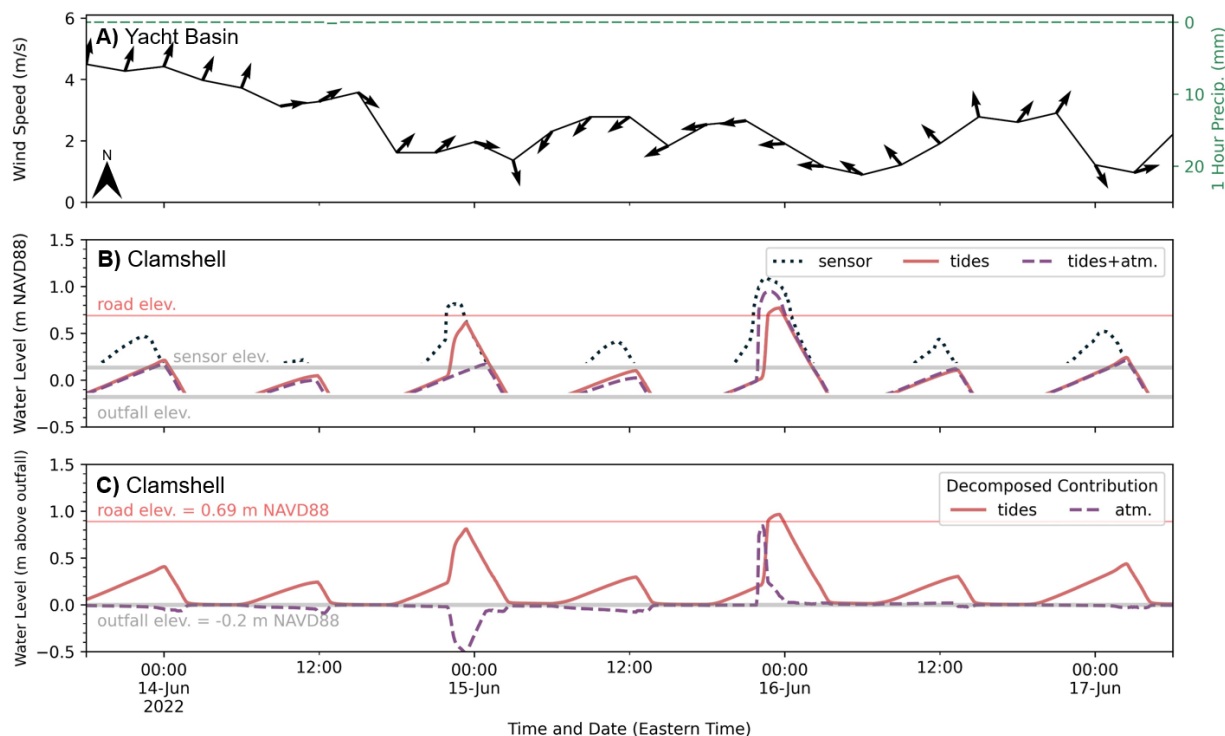


Figure 4. June 2022 perigean spring tide event. A) Measured 3-hr wind speed (left y-axis), wind direction (relative to north, arrows), and 1-hr precipitation (right y-axis) in the Yacht Basin. B) Measured (dotted) and modeled water levels at the Clamshell catch basin from simulations with different model forcing combinations. C) Decomposition of modeled water levels for tidal (solid line) and atmospheric (dashed line) contributions, relative to the outfall elevation of the Clamshell catch basin. Horizontal lines in (B-C) show elevation of the road (red line), catch basin outfall pipe (gray line), and water level sensor.

3.2.2 August 2022 rain event

Flooding during the August 2022 rain event was unexpected based on tidal predictions. Before and after the flood event, backflow prevention devices limited the amount of bay water entering the stormwater network at Clamshell Lane and Oystershell Lane during each high tide (Fig. 5B and C, respectively). On August 19, a rainfall event occurred during the rising tide (33 mm over two-hours, Fig. 5A). This event was a typical rainstorm; it was smaller than the one-year average recurrence interval for two-hour precipitation at Carolina Beach (56 mm; Bonnin et al., 2004). Flood depths on the roadway were small at both sensor locations (<0.2 m), but were larger at Oystershell Lane, which is higher in elevation.

Model simulations show the August 2022 rain event was driven by rainfall. Neither tides nor tides+atmospheric contributions elevated water levels in the Yacht Basin enough to flood the road at Clamshell (Fig. 5D) or Oystershell (Fig. 5E) Lane. However, the tides+atmospheric simulation shows that there was reduced capacity in both catch basins during the rainfall event due to the rising tide, impairing drainage of rainfall runoff to the Yacht Basin (Fig. 5B-C). The differing flood magnitudes and durations at the two sensor locations stem from a combination of differences in rainfall runoff draining to each catch basin (i.e., differences in tributary area and

the amount of impervious surfaces) and differences in stormwater capacity (i.e., how bay water impedes drainage through the network).

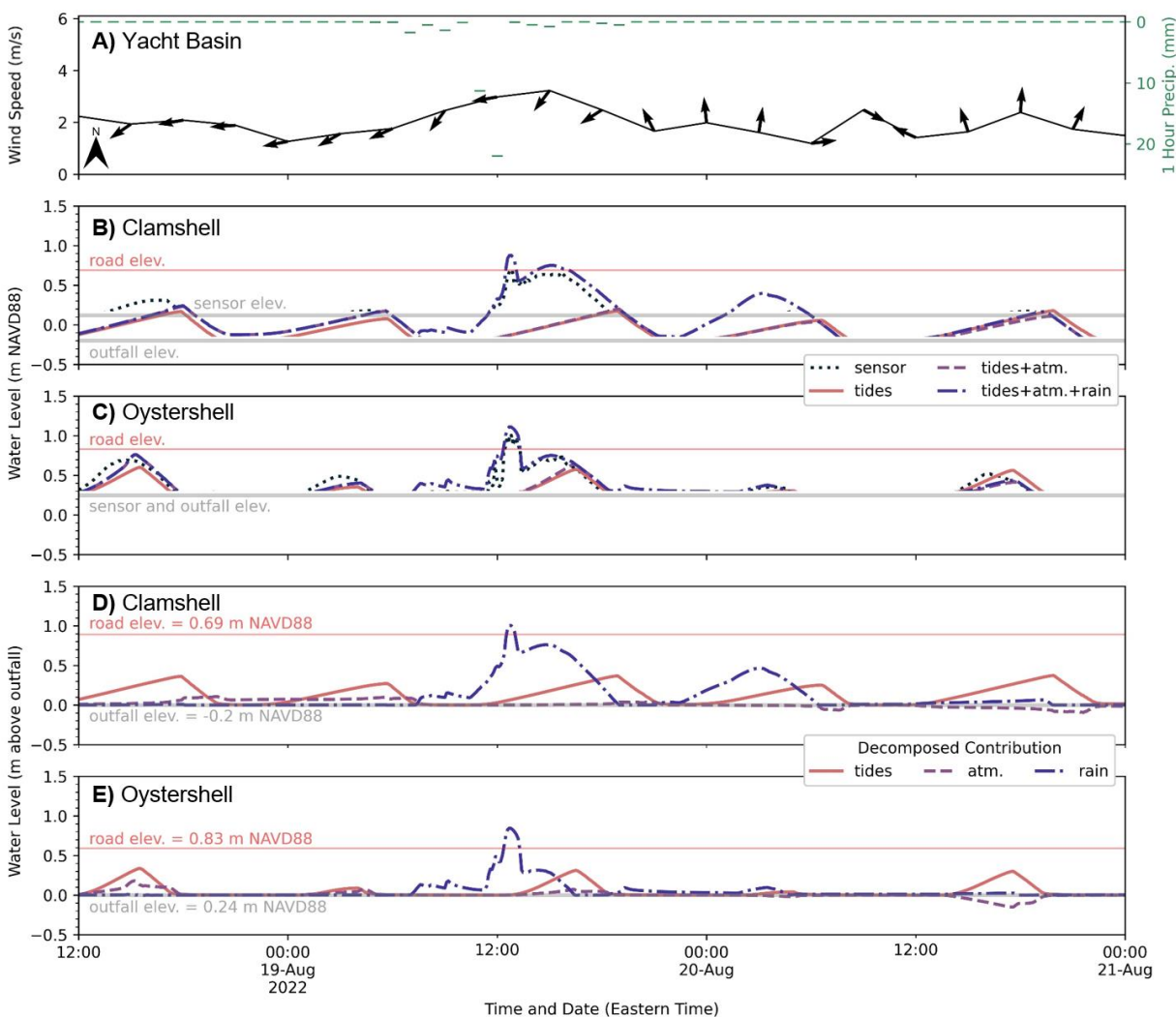


Figure 5. August 2022 rain event. A) Measured 3-hr wind speed (left y-axis), wind direction (relative to north, arrows), and 1-hr precipitation (right y-axis) in the Yacht Basin. B-C) Measured (dotted) and modeled water levels at the Clamshell (B) and Oystershell (C) catch basins from simulations with different model forcing combinations. D-E) Decomposition of modeled water levels for tidal (solid line), atmospheric (dashed line), and rainfall (dash-dot line) contributions, relative to the outfall elevation of the Clamshell (D) and Oystershell (E) catch basins.

3.2.3 January 2023 mixed-drivers event

On the morning of January 22, 2023, the Clamshell and Oystershell sensors measured floods that reached 0.4 m in magnitude and 4 hr in duration (Fig. 6B-C), which were the largest and longest floods of the three events examined through modeling. Prior to the flood, a low-pressure system located offshore Carolina Beach began moving north past the study site (Weather Forecast Office, 2023), producing a shift in wind from southwesterly to northeasterly at 00:00 on January 21 (Fig. 6A). Approximately 24 hours later, on the morning of January 22, the

1
2
3
4 offshore low produced a 48-mm, six-hour rain event (Fig. 6A). Like the August 2022 rain event,
5 this rainfall event was a relatively typical rainstorm; the one-year average recurrence interval for
6 six-hour precipitation in Carolina Beach is 75 mm (Bonnin et al., 2004).
7

8 Model simulations indicate that flooding would not have occurred at either sensor
9 location during the January 2023 mixed-drivers event due to tides alone (Fig. 6B-C, pink line);
10 only after incorporation of atmospheric effects and rain do simulation results approach observed
11 flood depths and durations (Fig. 6B-C, dash-dot blue line). Decomposition of atmospheric
12 contributions show that southwesterly winds prior to arrival of the offshore low produced a
13 setdown of water levels in the Yacht Basin (Fig. 6D-E, negative purple dashed line) through
14 January 20. With the arrival of the offshore low on January 21-22 and associated shift in wind
15 direction, atmospheric contributions to water levels reversed from negative to positive at both
16 catch basins (i.e., at 06:00 on Jan. 22 in Fig. 6D-E). Thereafter, tides compounded with
17 atmospheric effects to first reduce, and later eliminate, drainage capacity in the stormwater
18 system. At both sensor locations, the tide filled the Yacht Basin to near to the elevation of the
19 outfall (Fig. 6B-C, pink line). Rainfall commenced thereafter, and with reduced capacity in the
20 stormwater network, runoff overwhelmed the system and flooded the road (Fig. 6B-C, blue
21 dash-dot line). Rainfall contributions to water levels (above the outfall elevation) were largest at
22 both locations at this time (Fig. 6D-E, dash-dot blue line). Thereafter, the combined influence of
23 atmospheric effects and rising tides kept floodwaters on the road by eliminating stormwater
24 drainage capacity.
25
26
27
28
29

30 This compound sequence of three different flood drivers produced the fifth longest flood
31 on record (Fig. 3), longer than would have been expected considering any partial subset of
32 drivers. Rainfall also occurred during the next rising tide on the evening of January 22 (Fig. 6A),
33 but did not produce roadway flooding at either sensor location (Fig. 6B-C) as the tidal amplitude
34 was smaller than the previous tidal peak and atmospheric contributions were small (Fig. 6D-E).
35
36
37
38
39
40
41
42
43
44
45
46
47
48
49
50
51
52
53
54
55
56
57
58
59
60
61
62
63
64
65

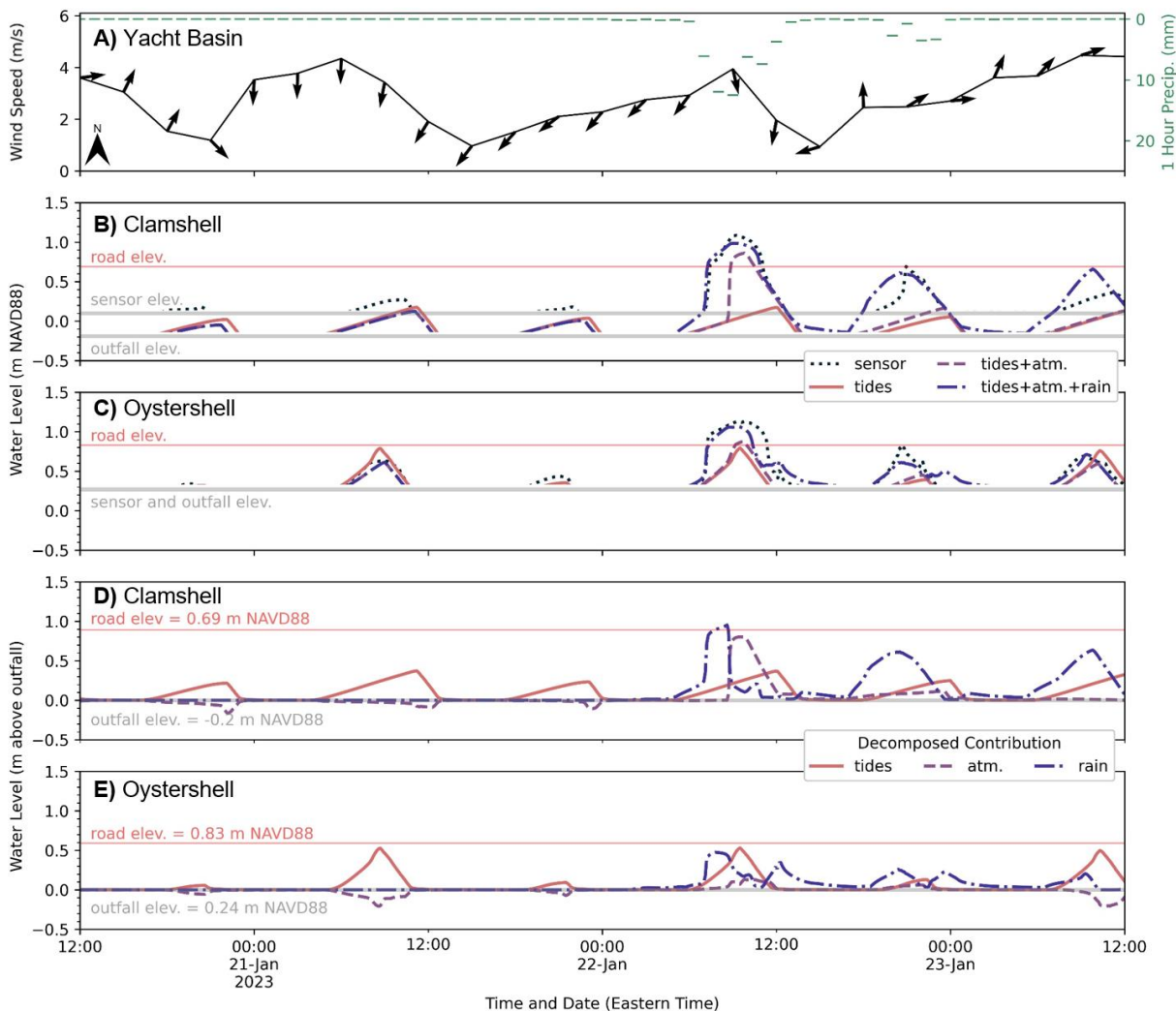


Figure 6. January 2023 mixed-drivers event. A) Measured 3-hr wind speed (left y-axis), wind direction (relative to north, arrows), and 1-hr precipitation (right y-axis) in the Yacht Basin. B-C) Measured (dotted) and modeled water levels at the Clamshell (B) and Oystershell (C) catch basins from simulations with different model forcing combinations. D-E) Decomposition of modeled water levels for tidal (solid line), atmospheric (dashed line), and rainfall (dash-dot line) contributions, relative to the outfall elevation of the Clamshell (D) and Oystershell (E) catch basins.

3.2.4 Flood spatial extents

The preceding analysis of flood drivers focused on individual sensor locations, where model simulations directly compare to flood measurements. In this section, we use the validated model to look beyond sensor locations and examine how non-tidal drivers compounded with tides to modify the spatial extent of modeled floods. We quantify changes in flood extent as an increase in inundated area and water volume relative to the tides simulations, calculated for the timestep with the maximum modeled flood depth at the Clamshell sensor. We limit our analysis to the north end of the Yacht Basin (in the proximity of the Clamshell sensor, Fig. 7), as this area is subject to both shoreline overtopping and stormwater network inundation.

1
2
3
4 The decomposition of flood drivers during the June 2022 perigean spring tide event
5 identified that atmospheric forcing (northeasterly winds) compounded with tides to produce
6 roadway flooding at the Clamshell sensor (Fig. 4). This compounding resulted in an increase in
7 inundated area and flood volume, beyond what would have been observed by tides alone, of
8 4300 m² and 1400 m³ (respectively, seen through comparison of Fig. 7A,B). The contribution
9 from wind setup allows for more overtopping of low-lying shorelines, which then floods the road
10 – first north of the Yacht Basin along Florida Avenue and then along Canal Drive – and
11 increases the connectivity of floodwaters in the road. (The patchiness of floodwaters in Fig. 7A
12 largely stems from flooding via stormwater network inundation by tides.)
13

14
15
16 The spatial pattern of flooding observed for the other two modeled events differ from the
17 June 2022 perigean spring tide event due to rainfall. For the August 2022 rain event and the
18 January 2023 mixed-drivers event, water accumulates along nearly all roads in this portion of
19 the study site because drainage of rainfall runoff via the stormwater network is impeded by bay
20 water levels that submerge stormwater outfalls to the Yacht Basin (shown during the time of
21 maximum modeled flood depth at the Clamshell sensor, Fig. 7E,H). Consistent with the findings
22 from the driver decompositions (Fig. 5 and 6), the compound nature of the events resulted in a
23 significant increase in flood volumes beyond what would be expected from tides alone (by 1600
24 m³ and 2900 m³, respectively; Fig. 7E,H).
25
26
27
28
29
30
31
32
33
34
35
36
37
38
39
40
41
42
43
44
45
46
47
48
49
50
51
52
53
54
55
56
57
58
59
60
61
62
63
64
65

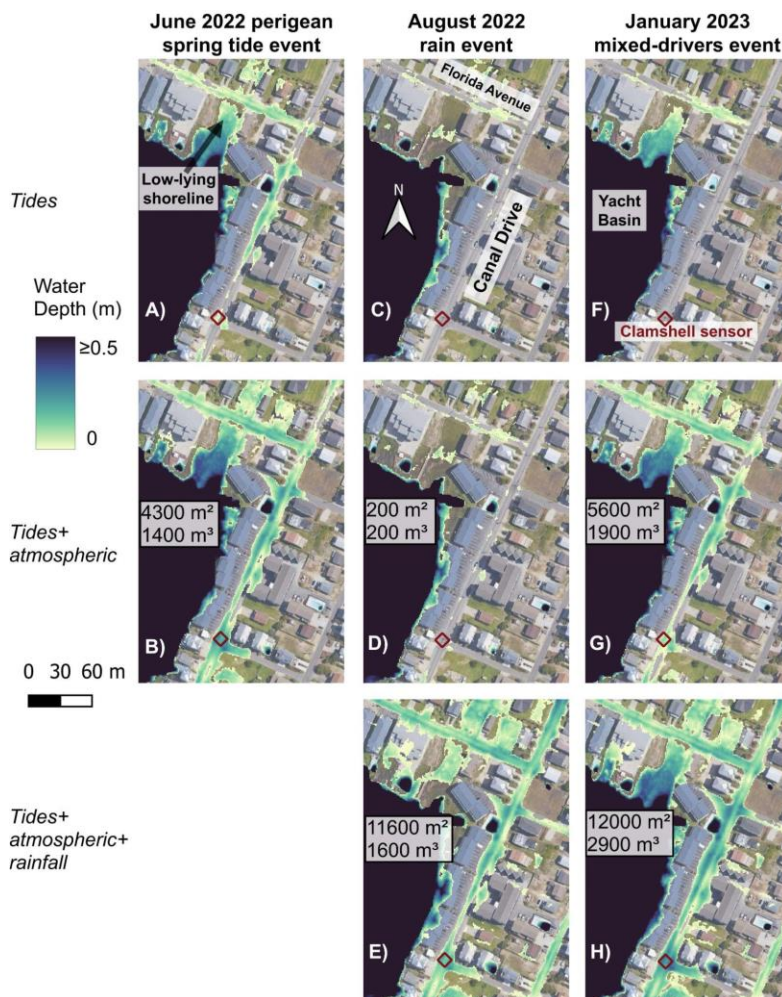


Figure 7. Simulated maximum flood extents and depths adjacent to the northeast corner of the Yacht Basin (see stormwater system in Fig. 1C). Columns show the three modeled flood events. Rows show the three model flood simulations with different model forcing combinations. Increases in inundated area (m²; top) and water volume (m³; bottom) within the plotted extents relative to each event's tides simulation are boxed in the tides+atmospheric and tides+atmospheric+rainfall (expect June 2022, no rain during this event) maps. Flood extents are extracted from the tides+atmospheric+rainfall simulation timestep with maximum modeled flood depth at the Clamshell sensor. A brown diamond indicates the location of the Clamshell sensor.

4. Discussion

In Carolina Beach, NC, we documented 46 floods in one year, highlighting the frequency of floods occurring outside of extreme storms (43 out of 46 floods) due to SLR. Building on the finding of Gold et al. (2023) that rain can compound with even moderate tides to produce coastal flooding due to impaired stormwater networks, we show that other non-tidal factors – namely wind, and the combination of wind, rain, and impaired stormwater networks – contribute to flood magnitude, extent, and duration during tidal floods, and consequently increase the frequency of flooding in low-lying coastal communities.

1
2
3
4 Wind was a major contributor to unexpected flooding in Carolina Beach, and localized
5 wind setup likely drives similar non-storm flooding in other bayside communities. During our
6 study period, 33% of chronic coastal floods (14 of 43 floods, all outside of extreme storms)
7 occurred during forecasted tides below the community's monitoring threshold (Fig. 3D). Eleven
8 of these 14 unexpected floods occurred during a rising or high tide accompanied by
9 northeasterly wind. Because Carolina Beach is backed by a narrow, shallow bay and
10 intracoastal channel (Fig. 1), even a small amount of sustained wind forcing can modify water
11 levels if winds are aligned with the longest fetch of the water body. Wind speeds during the
12 unexpected floods were below tropical wind forcing (2.2 - 6.8 m/s, averaged over the 24 hours
13 preceding the event), but because winds were out of the northeast and aligned with the Yacht
14 Basin, wind setup combined with tides to produce roadway flooding. Given that many
15 waterways and bays in North Carolina are oriented (along their longest axis) north to northeast,
16 and that non-tidal residuals have been shown to contribute significantly to marine water levels at
17 tide gauges (Li et al., 2022), this issue is likely widespread. More broadly, back bays are
18 common features along developed barrier coastlines globally, meaning wind contributions to
19 marine water levels in these embayed systems may significantly contribute to flooding, if not
20 now, then in the future with continued SLR.

21
22 Our results suggest that flood risk may be substantially underestimated when using
23 simpler models. The novel coupling between an ocean-scale hydrodynamic model and a 1D-2D
24 flow model introduced in this paper allows for simulation of flood contributions from marine
25 sources (tides, wind), land-based sources (rainfall), and infrastructure (stormwater, bulkheads)
26 at hyperlocal scales. Using this model, we find that wind can increase flood magnitudes,
27 durations (Fig. 4), and spatial extents (Fig. 7B), even during expected perigean spring tide
28 events. Wind and tides can also compound with rainfall to produce floods that are deeper and
29 longer in duration than would have otherwise occurred with individual drivers (Fig. 5-6), but flood
30 characteristics (magnitude and duration) vary spatially. The compounding of flood drivers and
31 their interactions that we capture cannot be resolved in bathtub flood models (e.g., Williams and
32 Lück-Vogel, 2020; Yunus et al., 2016), nor (non-coupled) hydrodynamic flood models (e.g.,
33 Sadler et al., 2020; Shen et al., 2019). Furthermore, the coupled flood model introduced in this
34 study could be extended to include other marine (e.g., wave setup, riverine flow) and land-
35 based processes (e.g., groundwater) that are not currently significant flood drivers in Carolina
36 Beach (see Supplement Section 2), but are suggested as drivers of chronic coastal floods
37 elsewhere (Moftakhari et al., 2017).

38
39 For coastal communities facing chronic flooding, considering factors beyond the tidal
40 forecast is critical for effective flood responses and mitigation. In Carolina Beach, 24-hr
41 sustained winds greater than 2.2 m/s (5 mph) out of the northeast often contribute to
42 unexpected floods (Fig. 3D); therefore, flood monitoring could be extended to include forecasts
43 of wind speeds and directions. Wind-driven contributions to flood extent during predicted high-
44 tide events also warrant consideration, as small amounts of wind (from the right direction) can
45 disproportionately enhance flooding in low-lying coastal areas (Fig. 7A-B). Finally, monitoring
46 could be extended to include forecasted rain events, particularly if they occur around tidal
47 peaks. However, monitoring of wind, rain, and tides – as well as the functionality of backflow
48 prevention devices (e.g., biofouling) – presents a significant challenge for local municipalities
49 with limited personnel. Alternatively, flood models, like that presented here, could be adapted to
50
51
52
53
54
55
56
57
58
59
60
61
62
63
64
65

run in a forecast capacity using existing inputs (tidal constituents and forecasted meteorological conditions). Model forecasts could provide spatially continuous predictions of flood depth, extent, and timing to inform community preparedness measures like road closures and alerts. Similarly, in-situ data within stormwater networks could be used during non-flood conditions to track the functionality of backflow prevention devices.

Chronic flooding will become more common in coastal communities worldwide with SLR (IPCC, 2022), and the drivers of these floods will likely change for individual communities; communities that today only flood during the highest high tides may soon need to plan for flooding from wind, rain, and impaired stormwater networks. A local understanding of flood drivers now and in the future is necessary to evaluate the effectiveness of potential flood mitigation strategies. In Carolina Beach, for example, backflow prevention devices installed on stormwater outfalls to the Yacht Basin are effective in preventing small floods from high bay water levels. However, flood prevention is compromised during higher water level events by low-lying shorelines elsewhere (water finds a way) or rainfall occurring at high tide (water has nowhere to go). Larger infrastructure interventions like raising shoreline elevations may change the relative importance of different flood drivers – for example, bulkheads or ring dykes may be effective at reducing flooding from marine-based drivers, but exacerbate flooding from rainfall and groundwater.

5. Conclusion

By combining in-situ measurements of flooding and a numerical model, we show that, due to SLR, non-tidal marine (localized wind setup) and land-based factors (rainfall, impaired stormwater networks) lead to flooding at hyperlocal (block-by-block) scales in low-lying coastal communities. These factors can also exacerbate the depth, duration, and extent of (predicted) high-tide floods. Our analysis focuses on the Town of Carolina Beach, NC, USA, which has features that are common to many coastal communities worldwide but is particularly low-lying and therefore a vanguard of what will occur elsewhere with increasing sea levels.

- For coastal communities adjacent to shallow bays: sustained wind – here, greater than 2.2 m/s (5 mph) – aligned with the longest axis of the bay elevates marine water levels locally during normal tidal cycles and contributes to flooding (modulating flood depths, extents, and durations).
- For communities with stormwater infrastructure at or below the high tide line: partial submergence of stormwater infrastructure (even when equipped with backflow prevention devices) by tides limits drainage such that even a minor rainstorm – here, 2-hr rain accumulation on the order of 5 to 35 mm – can lead to flooding.

Accounting for these additional land and marine-based factors in flood prediction presents challenges for communities with limited capacity to monitor weather and stormwater network performance. Models that can simulate compound interactions between multiple flood drivers and resolve stormwater infrastructure, like the coupled flood model presented here, can build predictive capacity by increasing understanding of flood drivers.

Acknowledgements

This work was supported by Institution Grant (NA22OAR4170109) to the NC Sea Grant Program from the National Sea Grant Office, National Oceanic and Atmospheric Administration. This material is also based upon work supported by the U.S. Department of Homeland Security under Grant Award Number 2015-ST-061-ND0001-01. The views and conclusions contained herein are those of the authors and should not be interpreted as necessarily representing the official policies, either expressed or implied, of the U.S Department of Homeland Security. Anarde was additionally supported by the Gulf Research Program Early-Career Research Fellowship (2000013691-2022). We thank the Town of Carolina Beach staff, especially Jeremy Hardison and Daniel Keating, for their collaboration. We also thank Anthony Whipple, Ryan McCune, Christine Baker, Tomás Cuevas López, Meagan Kittle-Autry, and Julia Harrison for feedback provided during the development of this paper, and Nicolette Volp and Olof Baltus for their guidance during 3Di model development.

Author contributions

Conceptualization: Katherine Anarde, Miyuki Hino, Casey Dietrich

Data curation: Thomas Thelen

Funding acquisition: Katherine Anarde, Miyuki Hino

Formal analysis: Thomas Thelen

Original writing: Thomas Thelen

Editing: Thomas Thelen, Katherine Anarde, Miyuki Hino, Casey Dietrich

References

- APTIM, 2019. Town of Carolina Beach Canal Drive Flooding & Vulnerability Assessment Study. Aptim Coastal Planning & Engineering of North Carolina.
- Asher, T.G., et al., 2019. Low frequency water level correction in storm surge models using data assimilation. *Ocean Model.* 144, 101483. <https://doi.org/10.1016/j.ocemod.2019.101483>
- Befus, K.M., et al., 2020. Increasing threat of coastal groundwater hazards from sea-level rise in California. *Nat. Clim. Change* 10, 946–952. <https://doi.org/10.1038/s41558-020-0874-1>
- Blanton, B.O., Luettich, R.A., 2008. North Carolina Coastal Flood Analysis System Model Grid Generation (No. TR-08-05). RENCi, North Carolina.
- Bonnin, G.M., et al., 2004. Precipitation-Frequency Atlas of the United States. Volume 2 Version 3.0. Delaware, District of Columbia, Illinois, Indiana, Kentucky, Maryland, New Jersey, North Carolina, Ohio, Pennsylvania, South Carolina, Tennessee, Virginia, West Virginia. NOAA atlas ; 14.
- Bosserelle, A.L., et al., 2022. Groundwater Rise and Associated Flooding in Coastal Settlements Due To Sea-Level Rise: A Review of Processes and Methods. *Earths Future* 10, e2021EF002580. <https://doi.org/10.1029/2021EF002580>
- Buckman, S.T., Sobhaninia, S., 2022. The Impact of Sea-Level Flooding on the Real Estate Development Community in Charleston SC: Results of a ULI Member Survey. *J. Sustain. Real Estate* 14, 4–20. <https://doi.org/10.1080/19498276.2022.2095699>
- Carr, M.M., et al., 2024. Fecal Bacteria Contamination of Floodwaters and a Coastal Waterway From Tidally- Driven Stormwater Network Inundation. *GeoHealth* 8, e2024GH001020. <https://doi.org/10.1029/2024GH001020>
- Casulli, V., 2009. A high-resolution wetting and drying algorithm for free-surface hydrodynamics. *Int. J. Numer. Methods Fluids* 60, 391–408. <https://doi.org/10.1002/fld.1896>
- Casulli, V., Stelling, G.S., 2013. A semi-implicit numerical model for urban drainage systems. *Int. J. Numer. Methods Fluids* 73, 600–614. <https://doi.org/10.1002/fld.3817>
- Casulli, V., Stelling, G.S., 2011. Semi-implicit subgrid modelling of three-dimensional free-surface flows. *Int. J. Numer. Methods Fluids* 67, 441–449. <https://doi.org/10.1002/fld.2361>
- Dietrich, J.C., et al., 2011. Hurricane Gustav (2008) Waves and Storm Surge: Hindcast, Synoptic Analysis, and Validation in Southern Louisiana. *Mon. Weather Rev.* 139, 2488–2522. <https://doi.org/10.1175/2011MWR3611.1>
- Dusek, G., et al., 2022. A novel statistical approach to predict seasonal high tide flooding. *Front. Mar. Sci.* 9.
- Fan, Y., et al., 2017. A Coupled 1D-2D Hydrodynamic Model for Urban Flood Inundation. *Adv. Meteorol.* 2017, e2819308. <https://doi.org/10.1155/2017/2819308>
- Gold, A., et al., 2023. Data From the Drain: A Sensor Framework That Captures Multiple Drivers of Chronic Coastal Floods. *Water Resour. Res.* 59, e2022WR032392. <https://doi.org/10.1029/2022WR032392>
- Gold, A.C., et al., Inundation of Stormwater Infrastructure Is Common and Increases Risk of Flooding in Coastal Urban Areas Along the US Atlantic Coast. *Earths Future* 10, e2021EF002139. <https://doi.org/10.1029/2021EF002139>
- Hague, B.S., et al., 2023. The Global Drivers of Chronic Coastal Flood Hazards Under Sea-Level Rise. *Earths Future* 11, e2023EF003784. <https://doi.org/10.1029/2023EF003784>
- Hauer, M.E., et al., 2023. Sea level rise already delays coastal commuters. *Environ. Res. Clim.* 2, 045004. <https://doi.org/10.1088/2752-5295/acf4b5>
- Hayden-Lowe, J., et al., 2022. sunny-day-flooding-project/tutorials: v1.0.1. <https://doi.org/10.5281/zenodo.7017187>
- Hino, M., et al., 2019. High-tide flooding disrupts local economic activity. *Sci. Adv.* 5, eaau2736. <https://doi.org/10.1126/sciadv.aau2736>
- IPCC, Intergovernmental Panel on Climate Change, 2022. Sea Level Rise and Implications for

- Low-Lying Islands, Coasts and Communities, in: *The Ocean and Cryosphere in a Changing Climate: Special Report of the Intergovernmental Panel on Climate Change*. Cambridge University Press, pp. 321–446.
- Ju, Y., et al., 2017. Planning for the Change: Mapping Sea Level Rise and Storm Inundation in Sherman Island Using 3Di Hydrodynamic Model and LiDAR, in: Thakuria, P. (Vonu), Tilahun, N., Zellner, M. (Eds.), *Seeing Cities Through Big Data: Research, Methods and Applications in Urban Informatics*, Springer Geography. Springer International Publishing, Cham, pp. 313–329. https://doi.org/10.1007/978-3-319-40902-3_18
- Li, S., et al., 2022. Contributions of Different Sea-Level Processes to High-Tide Flooding Along the U.S. Coastline. *J. Geophys. Res. Oceans* 127, e2021JC018276. <https://doi.org/10.1029/2021JC018276>
- Luetlich, R.A., et al., 1992. ADCIRC : an advanced three-dimensional circulation model for shelves, coasts, and estuaries. Report 1, Theory and methodology of ADCIRC-2DD1 and ADCIRC-3DL (Report). Coastal Engineering Research Center (U.S.).
- Macías-Tapia, A., et al., 2021. Effects of tidal flooding on estuarine biogeochemistry: Quantifying flood-driven nitrogen inputs in an urban, lower Chesapeake Bay sub-tributary. *Water Research*, 201, 117329. <https://doi.org/10.1016/j.watres.2021.117329>
- Moftakhari, H.R., et al., 2018. What Is Nuisance Flooding? Defining and Monitoring an Emerging Challenge. *Water Resour. Res.* 54, 4218–4227. <https://doi.org/10.1029/2018WR022828>
- Moftakhari, H.R., et al., 2017. Cumulative hazard: The case of nuisance flooding. *Earths Future* 5, 214–223. <https://doi.org/10.1002/2016EF000494>
- Mydlarz, C., et al., 2024. FloodNet: Low-Cost Ultrasonic Sensors for Real-Time Measurement of Hyperlocal, Street-Level Floods in New York City. *Water Resour. Res.* 60, e2023WR036806. <https://doi.org/10.1029/2023WR036806>
- NOAA, National Oceanic and Atmospheric Administration, 2022. Wrightsville Beach, NC - Station ID: 8658163.
- Office for Coastal Management, 2022. 2015-2017 C-CAP Derived 10 meter Land Cover - BETA.
- Rogers, E., et al., 2009. The NCEP North American mesoscale modeling system: Recent changes and future plans.
- Sadler, J.M., et al., 2020. Exploring real-time control of stormwater systems for mitigating flood risk due to sea level rise. *J. Hydrol.* 583, 124571. <https://doi.org/10.1016/j.jhydrol.2020.124571>
- Seyoum, S.D., et al., 2012. Coupled 1D and Noninertia 2D Flood Inundation Model for Simulation of Urban Flooding. *J. Hydraul. Eng.* 138, 23–34. [https://doi.org/10.1061/\(ASCE\)HY.1943-7900.0000485](https://doi.org/10.1061/(ASCE)HY.1943-7900.0000485)
- Shen, Y., et al., 2019. Flood risk assessment and increased resilience for coastal urban watersheds under the combined impact of storm tide and heavy rainfall. *J. Hydrol.* 579, 124159. <https://doi.org/10.1016/j.jhydrol.2019.124159>
- Silverman, A. I., et al., 2022. Making waves: Uses of real-time, hyperlocal flood sensor data for emergency management, resiliency planning, and flood impact mitigation. *Water Research*, 220, 118648. <https://doi.org/10.1016/j.watres.2022.118648>
- Stelling, G.S., 2012. Quadtree flood simulations with sub-grid digital elevation models. *Proc. Inst. Civ. Eng. Water Manag.* 165, 567–580.
- Sweet, W., et al., 2018. Patterns and projections of high tide flooding along the U.S. coastline using a common impact threshold.
- Sweet, W., et al., 2022. Global and Regional Sea Level Rise Scenarios for the United States: Updated Mean Projections and Extreme Water Level Probabilities Along U.S. Coastlines (No. NOAA Technical Report NOS 01). National Oceanic and Atmospheric Administration, National Ocean Service, Silver Spring, MD.
- Thatcher, C.A., et al., 2016. Creating a Coastal National Elevation Database (CoNED) for

- 1
2
3
4 Science and Conservation Applications. *J. Coast. Res.* 64–74.
5 <https://doi.org/10.2112/SI76-007>
6 Thiéblemont, R., et al., 2023. Chronic flooding events due to sea-level rise in French Guiana.
7 *Sci. Rep.* 13, 21695. <https://doi.org/10.1038/s41598-023-48807-w>
8 Volp, N.D., et al.. A finite volume approach for shallow water flow accounting for high-resolution
9 bathymetry and roughness data. *Water Resour. Res.* 49, 4126–4135.
10 <https://doi.org/10.1002/wrcr.20324>
11 Weather Forecast Office: Newport/Morehead City, NC, 2023. Eastern North Carolina Monthly
12 Climate Report: January 2023.
13 Westerink, J.J., et al., 1992. Tide and Storm Surge Predictions Using Finite Element Model. *J.*
14 *Hydraul. Eng.* 118, 1373–1390. [https://doi.org/10.1061/\(ASCE\)0733-](https://doi.org/10.1061/(ASCE)0733-9429(1992)118:10(1373))
15 [9429\(1992\)118:10\(1373\)](https://doi.org/10.1061/(ASCE)0733-9429(1992)118:10(1373))
16 Williams, L.L., Lück-Vogel, M., 2020. Comparative assessment of the GIS based bathtub model
17 and an enhanced bathtub model for coastal inundation. *J. Coast. Conserv.* 24, 23.
18 <https://doi.org/10.1007/s11852-020-00735-x>
19 Yunus, A.P., et al., 2016. Uncertainties in Tidally Adjusted Estimates of Sea Level Rise Flooding
20 (Bathtub Model) for the Greater London. *Remote Sens.* 8, 366.
21 <https://doi.org/10.3390/rs8050366>
22 Zahura, F.T., Goodall, J.L., 2022. Predicting combined tidal and pluvial flood inundation using a
23 machine learning surrogate model. *J. Hydrol. Reg. Stud.* 41, 101087.
24 <https://doi.org/10.1016/j.ejrh.2022.101087>
25
26
27
28
29
30
31
32
33
34
35
36
37
38
39
40
41
42
43
44
45
46
47
48
49
50
51
52
53
54
55
56
57
58
59
60
61
62
63
64
65

1 *Supplement*2 *1. ADCIRC simulation validation*

3 We compare ADCIRC simulation results with field data. The ADCIRC model results
 4 include a time series of water levels reported at one-minute intervals in the Yacht Basin. The
 5 Yacht Basin weather station and water level sensor maintained by the Town of Carolina Beach
 6 provides field water level data. We show three time series for each flood event: 1) water levels
 7 measured at the weather station, 2) an ADCIRC simulation with only tidal forcing, and 3) an
 8 ADCIRC simulation with tidal and atmospheric forcing. Table S.1 presents the root-mean-
 9 square error (RMSE) calculated by comparing the measured water levels to the tides and
 10 tides+atmospheric simulations. For each event, the tides+atmospheric simulation has an RMSE
 11 that is less than or equal to the tides simulation, indicating that the tides+atmospheric
 12 simulations were more accurate to measured water levels than the tides simulations.

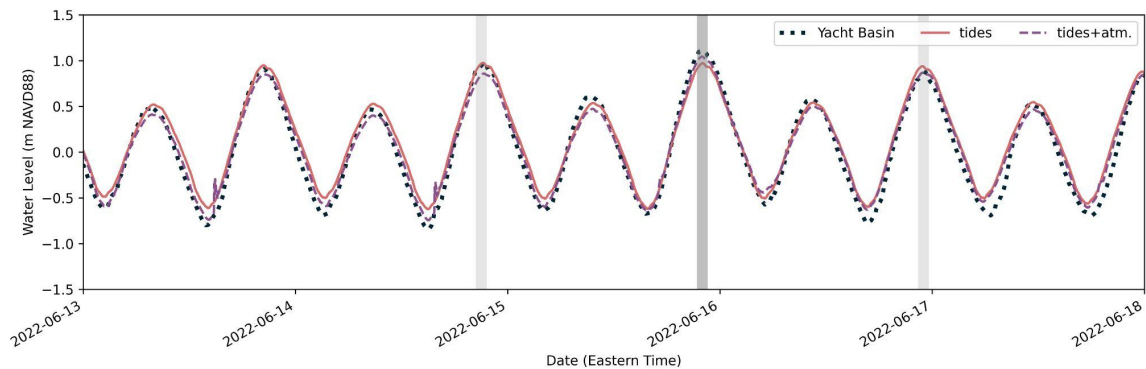
13
 14 Table S.1. RMSE (m) between time series of measured water levels from the Yacht Basin
 15 weather station and ADCIRC simulation results from the Yacht Basin with tides and
 16 tides+atmospheric forcing.

Flood event		June 2022 perigean spring tide event	August 2022 rain event	January 2023 mixed-drivers event
<i>RMSE (m): simulation vs. measurements</i>	<i>tides</i>	0.14	0.14	0.22
	<i>tides+atmospheric</i>	0.10	0.14	0.13

17
 18 Figure S.1 presents the Yacht Basin modeled and measured time series from the June
 19 2022 perigean spring tide event. Measured water levels show a 2 m tidal range, one of the
 20 largest tidal ranges of the year (NOAA, 2022). On the evening of June 15 (figure S.1, dark gray),
 21 the measured high tide is about 0.2 m higher than other measured high tides and the peak
 22 water level in the tides simulation. The small relative change in the tides simulation peaks on
 23 June 14 (figure S.1, light gray), 15, and 16 (figure S.1, light gray) suggests that this 0.2 m bump
 24 is not tidally driven. The tides+atmospheric simulation time series is depressed by atmospheric
 25 conditions below the tides simulation on all days except June 15-16, when the trend reverses.
 26 Here, the tides+atmospheric results simulate peak water levels on June 15 to within 0.03 m.
 27 This result indicates an atmospheric contribution to high water levels on June 15 that is
 28 captured by the tides+atmospheric simulation.

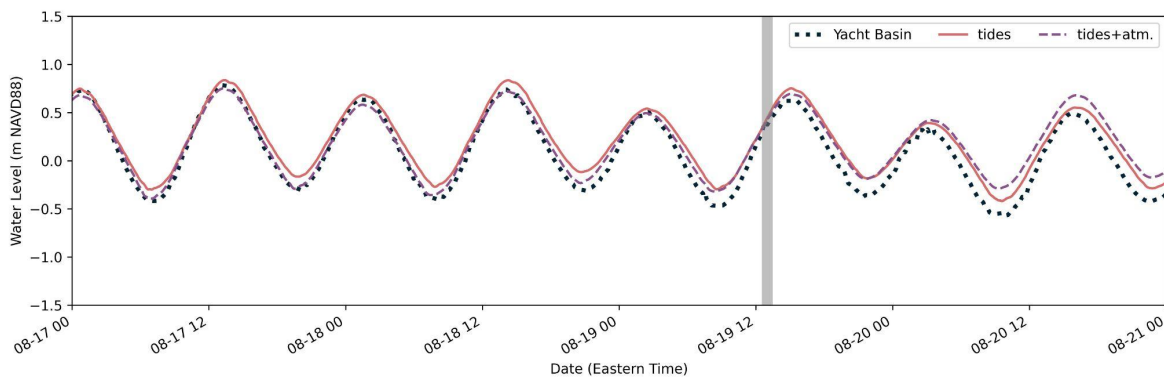
29 The June 2022 perigean spring tide event (figure S.1) and January 2023 mixed-drivers
 30 event (figure S.3) modeled time series show some sharp peaks at the lowest simulation water
 31 levels. This variability in the simulation is caused by ADCIRC node wetting and drying
 32 instabilities far from our study site. In this case, our simulation shows a buildup of high water in
 33 the Intracoastal Waterway 50 km north of Carolina Beach. The sudden change of several
 34 computational nodes from dry to wet at this location generates a pulse of water that travels
 35 down the Intracoastal Waterway to Carolina Beach. While this simulated pulse is not
 36 representative of reality, it occurs only at the lowest water level conditions. The wet/dry

1 instability does not affect our analysis of flooding because flooding occurs at water levels more
 2 than a meter higher than the water levels that trigger the instability.
 3



4
 5 Figure S.1. June 2022 perigean spring tide event Yacht Basin water levels. The dotted line
 6 denotes water levels measured at the Yacht Basin weather station. The red solid line shows
 7 water levels from an ADCIRC simulation with tidal forcing.
 8

9 Figure S.2 presents the modeled and measured water level time series around the
 10 August 2022 rain event. During this event, roadway flooding would not have occurred without
 11 the rainfall that took place at mid-tide. The tidal range during this time was about 1.5 m, 0.5 m
 12 smaller than the June 2022 perigean spring tide event. In this time series, we see minimal
 13 difference between the tides and tides+atmospheric ADCIRC simulations. This similarity
 14 indicates benign atmospheric conditions that neither depress nor elevate water levels in the
 15 Yacht Basin. While a rain event occurs and causes flooding on August 19 (Figure S.2, gray
 16 background), this flood does not co-occur with atmospheric conditions that alter tidally-driven
 17 water levels by more than 0.1 m. This finding agrees with previous research demonstrating that
 18 peak contributions of non-tidal residual to chronic flooding in North Carolina occur more often in
 19 the fall and winter (Li et al., 2022) and less often in the summer. In our case study, the winter
 20 January 2023 mixed-drivers event features larger atmospheric contributions (part of the non-
 21 tidal residual) than the summer June and August flood events.
 22

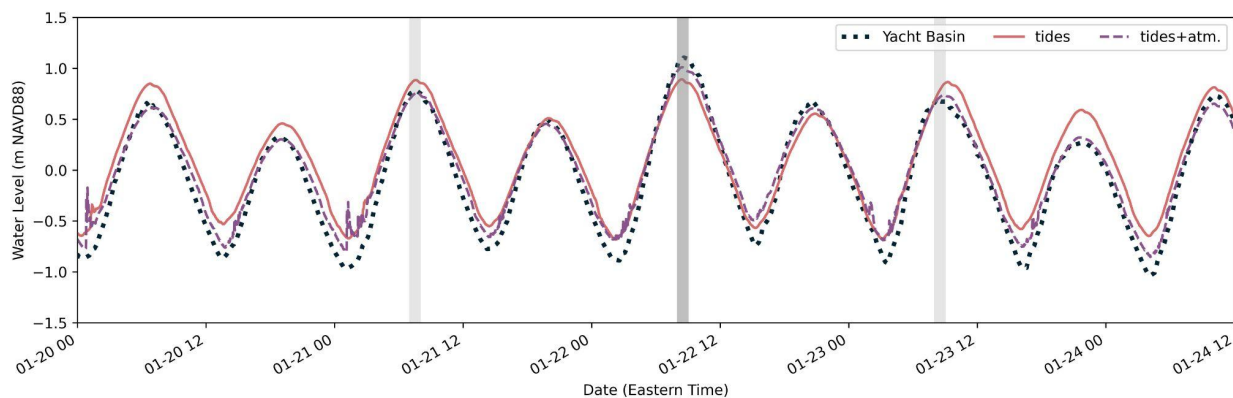


23
 24 Figure S.2. Yacht Basin measured (dotted) and ADCIRC modeled (tides: solid red;
 25 tides+atmospheric: purple dashed) water levels surrounding the August 2022 rain event. The
 26 flood event took place during the portion of the time series with the gray background.

1
2 Figure S.3 presents the Yacht Basin modeled and measured time series from the
3 January 2023 mixed-drivers event. The tidal range for the January 2023 flood event is less than
4 the June 2022 perigean spring tide event but greater than the August 2022 rain event. The
5 difference between the tides and tides+atmospheric simulation time series is greatest for the
6 January 2023 mixed-drivers event, indicating greater atmospheric influence on water levels. The
7 RMSE for the tides simulation relative to gauge data is 0.22 m, compared to 0.13 m for the
8 tides+atmospheric simulation. Furthermore, the tides+atmospheric RMSE is skewed higher by
9 the low water level spikes; therefore, the tides+atmospheric high water level results, the portion
10 of the time series where flooding occurs, is more accurate than the 0.13 m simulation RMSE
11 indicates.

12 The most interesting feature of this water level time series is the inversion of peak water
13 levels between January 21 and January 23 (Figure S.3, light gray) from the two ADCIRC
14 simulations. During peak water levels on January 21, the ADCIRC tides simulation peak is
15 higher than the tides+atmospheric simulation peak. However, this trend reverses on January 22
16 (Figure S.3, dark gray), when the tides+atmospheric simulation peak rises 0.15 m above the
17 tides peak. By January 23, the tides simulation peak is once again higher than the
18 tides+atmospheric simulation. On all three days, the tides+atmospheric simulation is more
19 closely aligned with gauge results compared to the tides simulation, exemplifying how our multi-
20 driver simulation framework captures multiple sources of water level contributions.

21



22
23 Figure S.3. Yacht Basin measured (dotted) and ADCIRC modeled (tides: solid red;
24 tides+atmospheric: purple dashed) water levels surrounding the January 2023 mixed-drivers
25 event. An atmospheric-driven increase in water levels is evident across the water level peaks
26 with gray background shading.

27

28 2. Flooding driver sensitivity testing

29 The complex hydrodynamic setting surrounding Carolina Beach compels an
30 investigation of processes other than tides, atmospheric effects, and rainfall runoff that could
31 drive flooding. We tested two other potential flooding drivers, riverine flow and wave setup – the
32 increase in water level driven by wave breaking – by assessing the sensitivity of water levels in
33 the Yacht Basin to these drivers.

1 We analyzed the sensitivity of water levels in Carolina Beach to flow in the Cape Fear
2 River by implementing a river discharge boundary condition in the ADCIRC model. This riverine
3 boundary condition is located at the United States Geological Survey monitoring location
4 02105769, the farthest downstream streamflow gauge on the main branch Cape Fear River. We
5 calculated the difference in simulated Yacht Basin water levels between a zero-flow boundary
6 condition and a constant river flow boundary condition (400 m³/s) that is greater than the peak
7 seven-day-average river discharge in 2022. For comparison, the mean annual flow at this gauge
8 is 147 m³/s with a standard deviation of 57 m³/s (Granato et al., 2017). The difference in Yacht
9 Basin water levels between the zero and 400 m³/s flow simulations was less than 0.05 m.
10 Therefore, we conclude that riverine flow is not a substantial chronic flooding driver in Carolina
11 Beach, and we do not use a river discharge boundary condition in our ADCIRC model.
12 However, the model framework developed here could simulate river contributions to local water
13 levels if it was implemented at a site where fluvial contributions to flooding are significant.

14 We also examined the contribution of wave setup to water levels in Carolina Beach.
15 Wave setup is considered in tightly coupled SWAN+ADCIRC (Dietrich et al., 2011). The SWAN
16 (Simulating WAVes Nearshore; Booij et al., 1999) model uses wind velocities from an
17 atmospheric dataset and water depths plus velocities calculated by ADCIRC as inputs to the
18 action balance equation describing wave evolution. Radiation stress gradients calculated in
19 SWAN are applied as surface stress in ADCIRC such that SWAN+ADCIRC simulations include
20 the contributions of waves to water levels and currents. We find that water levels in the Yacht
21 Basin differ by less than 0.01 m between SWAN+ADCIRC and ADCIRC simulations run on the
22 same mesh with the same wind forcing. Therefore, we conclude that wave setup is not a
23 substantial driver of chronic flooding in Carolina Beach.

24

25 3. ADCIRC water level offset calculation

26 Our use of ADCIRC solves for circulation driven by tides and atmospheric (wind and
27 pressure) forcing. However, there are other ocean-scale circulation drivers of coastal water
28 levels that ADCIRC cannot resolve. For example, thermal expansion of ocean water and major
29 ocean currents like the Gulf Stream are not resolved in ADCIRC. These unresolved processes
30 typically vary over longer time scales than tidal and atmospheric forcings that vary from hour to
31 hour (Asher et al., 2019). To account for the effects of unresolved forcings on coastal water
32 levels, we apply a spatially constant water level offset throughout the ADCIRC domain. This
33 technique follows methods used in previous ADCIRC studies (e.g., Westerink et al., 2008), with
34 the calculation adjusted slightly to work with the data available in Carolina Beach. We calculate
35 the global water level offset (ADCIRC parameter name: sea_surface_height_above_geoid)
36 according to the formula shown in Equation S.1. By subtracting averages of the tidal and
37 atmospheric simulation from measured water levels in the Yacht Basin, we isolate contributions
38 to Yacht Basin water levels that are neither tidal nor atmospheric. The twenty-day averaging
39 window was determined through sensitivity testing to provide the best fit to measured data
40 during the three simulated flood events. Importantly, since this method uses data from the
41 twenty days before a flood event, it could be used not only for hindcast simulations, but also in a
42 forecast scenario.

43

44

$$\bar{z}_{measured} - \bar{z}_{ADCIRC,tides+atm.} = z_{offset}$$

Equation S.1. Formula used to calculate the global water level offset in ADCIRC that accounts for seasonal water level fluctuations not captured in tidal or atmospheric forcings. \bar{z} are measured or modeled Yacht Basin water levels averaged over the 20 days preceding a flood. $\bar{z}_{measured}$ is calculated from water level measurements recorded at the Yacht Basin weather station. $\bar{z}_{ADCIRC,tides+atm.}$ is calculated from an ADCIRC simulation (without a global water level offset) run with tidal and atmospheric forcing. z_{offset} is the global water level offset value used in the ADCIRC portion of coupled flood model simulations.

4. 3Di weir loss coefficient tuning

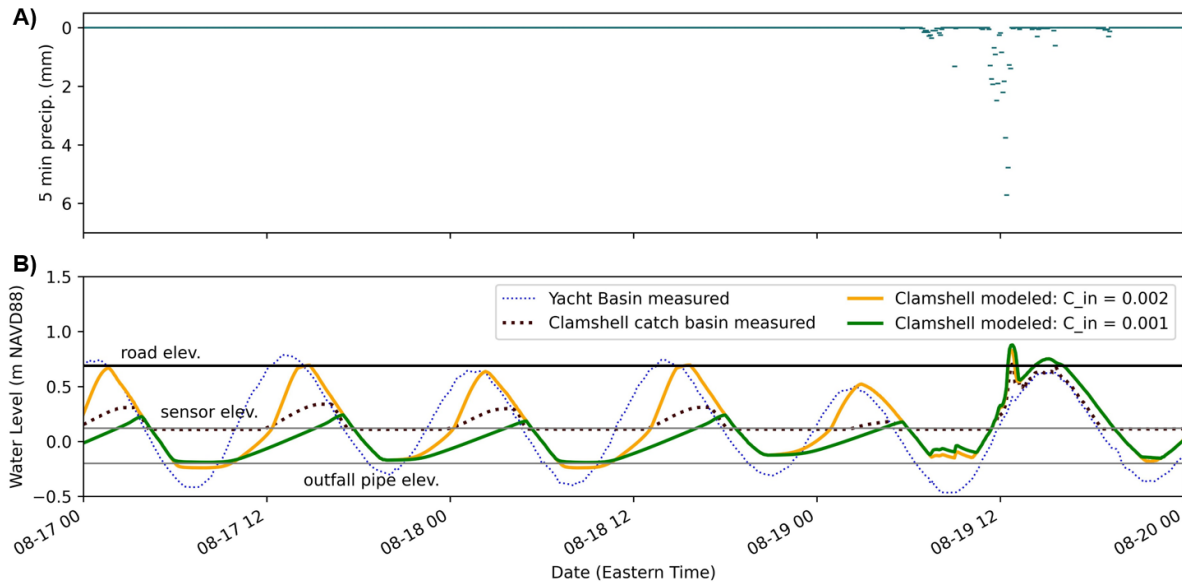
Weir flow in 3Di is calculated by solving a conservation of energy balance at the weir structure. The 3Di weir discharge formulation (Equation S.2) contains a discharge coefficient that we tune to match modeled water levels at the Clamshell and Oystershell stormwater outfalls to water levels measured by our sensors. We use different discharge coefficients for flows entering or exiting the stormwater system as shown in Table S.2 because backflow prevention devices have different effects on flows in different directions. Figure S.4 shows two examples of modeled discharge coefficients tested during coefficient tuning. Small coefficients produce a relatively slow flow entering the stormwater system (i.e., via leakage through the backflow prevention device or groundwater bypassing of the device), while larger coefficients mean that flow exits the stormwater system largely unimpeded (i.e., as dictated by the energy head balance at the outfall).

$$Q = CWg^{0.5}\left(\frac{2}{3}h\right)^{1.5}$$

Equation S.2. Weir flow (Q) formula solved by 3Di, where (C) is the tuned discharge coefficient, (W) is the cross-section width (equivalent to outfall pipe diameter), (g) is gravitational acceleration, and (h) is the water height above the weir crest level (in our case, the outfall pipe elevation).

Table S.2. Weir equation discharge coefficients used in 3Di simulations for flow through the Clamshell and Oystershell stormwater outfalls.

Catch basin	Discharge coefficient	
	For flow into stormwater system	For flow out of stormwater system
Clamshell	0.001	0.9
Oystershell	0.003	0.7



1
 2 Figure S.4. Comparison between two different modeled weir discharge coefficients for flow into
 3 the Clamshell catch basin. The 0.001 coefficient simulation result (green line) is a better match
 4 for the measured catch basin water levels (brown dotted line) than the 0.002 coefficient result
 5 (orange line). Note that the backflow prevention device keeps catch water levels below Yacht
 6 Basin levels (small dotted blue line) except when the catch basin fills from runoff during the rain
 7 event on August 19.

8
 9 5. Flood event photos



10
 11 Figure S.5. August 2022 rain event as seen from the Oystershell SuDS camera at 11:48
 12 Eastern Standard Time. A car drives through the floodwaters because Canal Drive was not
 13 closed during this flood.

1



2
3
4
5
6

Figure S.6. January 2023 mixed-drivers event as seen from the Oystershell SuDS camera at 09:18 Eastern Standard Time. Note the gate lowered to close Canal Drive on the left side of the image.



7
8
9
10
11

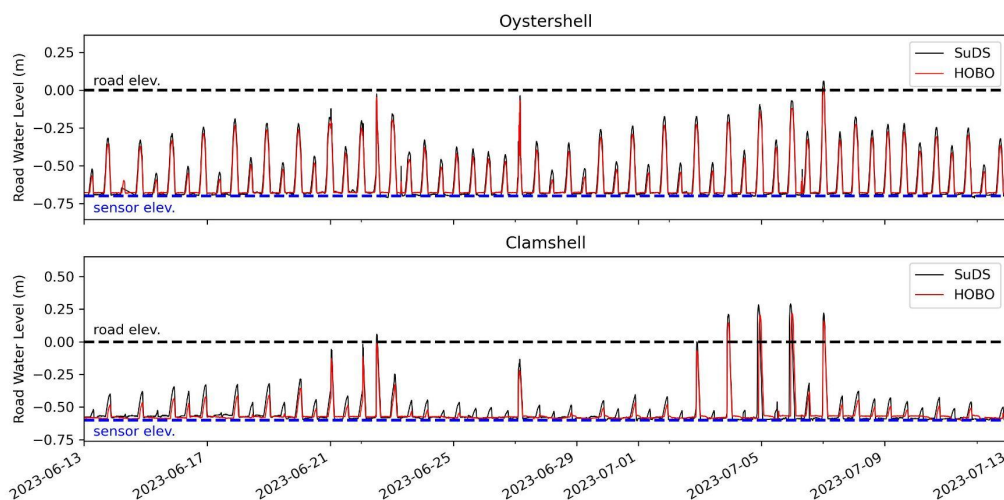
Figure S.7. January 2023 mixed-drivers event as seen from the Clamshell SuDS camera at 09:06 Eastern Standard Time.



1
2 Figure S.8. June 2022 perigean spring tide event as seen from Clamshell SuDS camera on
3 June 15 at 21:36 Eastern Standard Time. The photo shows the same field of view as Fig S.7.
4 Note the lights reflecting off the floodwaters.

5
6 **6. Sunny Day Flooding Sensor Validation**

7 We deployed HOBO data loggers at the same measurement location and elevation as
8 the Clamshell and Oystershell SuDS from May through July 2022. Here we zoom in on a one-
9 month period during the HOBO deployment when we collected data from both Sunny Day
10 Flooding Sensors (SuDS) for comparison with HOBO measurements. Figure S.9 compares
11 pressure measurements from the SuDS and HOBO adjusted for atmospheric pressure and
12 converted to water levels relative to the edge of road elevation. The RMSE for the Oystershell
13 and Clamshell SuDS measurements compared to HOBO measurements are 0.033 m and 0.060
14 m respectively.



15
16 Figure S.9. Comparison of one month of water levels measured by HOBO (red) and SuDS
17 (black) pressure loggers co-located at the Oystershell and Clamshell storm drains.

1 7. *Time periods with continuous water level data*

2

3 Table S.3. Summary of continuous water level measurement records during the study period
 4 (April 1, 2022 to April 24, 2023) with no sensor outages (i.e., no data gaps greater than 24
 5 hours) at the Clamshell and Oystershell sensors. Image records were nearly complete (less
 6 than 10 days of missed imagery between the two sensors).

Sensor Location	Time periods with water level measurements (year: month/date)
<i>Clamshell</i>	2022: 4/1 - 5/3; 5/13 - 5/17; 6/1 - 7/1; 7/13 - 7/19; 8/16 - 11/8; 11/10 - 12/11; 12/13 - 12/23; 2023: 1/8 - 1/16; 1/17 - 4/24
<i>Oystershell</i>	2022: 6/2 - 7/5; 7/13 - 7/30; 8/1 - 9/10; 9/11 - 11/8; 11/14 - 12/30 2023: 1/20 - 3/3

7

1 **References**

- 2 Asher, T.G., Luettich Jr., R.A., Fleming, J.G., Blanton, B.O., 2019. Low frequency water level
3 correction in storm surge models using data assimilation. *Ocean Model.* 144, 101483.
4 <https://doi.org/10.1016/j.ocemod.2019.101483>
- 5 Booij, N., Ris, R.C., Holthuijsen, L.H., 1999. A third-generation wave model for coastal regions:
6 1. Model description and validation. *J. Geophys. Res. Oceans* 104, 7649–7666.
7 <https://doi.org/10.1029/98JC02622>
- 8 Dietrich, J.C., Zijlema, M., Westerink, J.J., Holthuijsen, L.H., Dawson, C., Luettich, R.A., Jensen,
9 R.E., Smith, J.M., Stelling, G.S., Stone, G.W., 2011. Modeling hurricane waves and
10 storm surge using integrally-coupled, scalable computations. *Coast. Eng.* 58, 45–65.
11 <https://doi.org/10.1016/j.coastaleng.2010.08.001>
- 12 Granato, G.E., Ries III, K.G., Steeves, P.A., 2017. Compilation of streamflow statistics
13 calculated from daily mean streamflow data collected during water years 1901–2015 for
14 selected U.S. Geological Survey streamgages (USGS Numbered Series No. 2017–
15 1108), Compilation of streamflow statistics calculated from daily mean streamflow data
16 collected during water years 1901–2015 for selected U.S. Geological Survey
17 streamgages, Open-File Report. U.S. Geological Survey, Reston, VA.
18 <https://doi.org/10.3133/ofr20171108>
- 19 Li, S., Wahl, T., Barroso, A., Coats, S., Dangendorf, S., Piecuch, C., Sun, Q., Thompson, P.,
20 Liu, L., 2022. Contributions of Different Sea-Level Processes to High-Tide Flooding
21 Along the U.S. Coastline. *J. Geophys. Res. Oceans* 127, e2021JC018276.
22 <https://doi.org/10.1029/2021JC018276>
- 23 NOAA, National Oceanic and Atmospheric Administration, 2022. Wrightsville Beach, NC -
24 Station ID: 8658163.
- 25 Westerink, J.J., Luettich, R.A., Feyen, J.C., Atkinson, J.H., Dawson, C., Roberts, H.J., Powell,
26 M.D., Dunion, J.P., Kubatko, E.J., Pourtaheri, H., 2008. A Basin- to Channel-Scale
27 Unstructured Grid Hurricane Storm Surge Model Applied to Southern Louisiana. *Mon.*
28 *Weather Rev.* 136, 833–864. <https://doi.org/10.1175/2007MWR1946.1>